Essay: Pushing the Frontiers of High Energy Density Science toward Unexplored States of Matter

Federica Coppari*
Lawrence Livermore National Laboratory, Livermore, California, 94550, USA

(Received 27 May 2026; published 20 July 2026)

Recent breakthroughs in high energy density (HED) science, the study of materials at extreme conditions of pressure and temperature, are profoundly reshaping our understanding across multiple scientific fields. HED science encompasses extreme states of matter across plasma physics, warm dense matter, and condensed matter, bridging fields such as planetary science, materials science, and fusion energy research. Enabled by revolutionary technologies such as ultraintense laser-driven compression, novel insights are emerging from continuous developments. Historically anchored in plasma science, HED physics is evolving toward the understanding of new states of matter, following technological advances. In this Essay, I will present my view of HED science, with particular emphasis on a relatively new and unexplored area within the field that extends beyond plasma physics and warm dense matter, and includes condensed solid and liquid matter at extreme densities and (relatively) cold temperatures.

Part of a series of Essays which concisely present author visions for the future of their field.

DOI: 10.1103/1d8y-2cmz

Introduction—High energy density (HED) science explores the behavior of materials under extreme pressure and temperature conditions, like those found deep inside planets and stars, fusion reactions, and nuclear events. At HED conditions, materials properties differ dramatically from those at ambient pressure and room temperature, due to significant changes in the forces between atoms and electrons as matter is compressed and heated. The boundaries of the HED regime are loosely defined, spanning a wide range of states, from plasma to warm dense matter (WDM) to condensed matter.

HED physics [1,2] deals with materials at pressure greater than 100 GPa (equivalent to 1 Mbar). Because pressure has the units of energy density, the onset of the HED regime has been associated with a value of order 10^{11} J/m^3. For an ideal monatomic gas, pressure and energy are directly proportional, differing only by a factor of order unity. However, in real HED systems, such as partially ionized plasmas, WDM, and dense solids, the total internal energy includes significant contributions from ionization, electron degeneracy, and interatomic potential energy. As a result, the energy density does not directly map into the pressure of the system. Therefore, even though pressure is a convenient mechanical metric for identifying HED regimes, in general, it should not be interpreted as a direct measure of stored energy density. This point is illustrated in Fig. 1, which shows energy density contours

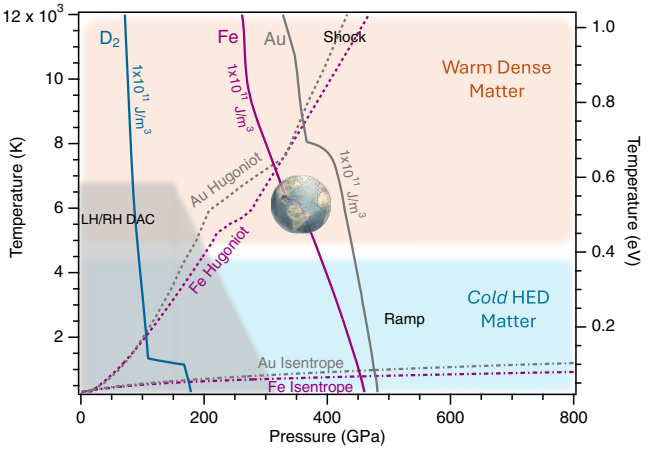


FIG. 1. Temperature-pressure diagram showing the 1×10^{11} J/m^3 energy density contours (solid lines) for deuterium [3] (navy), iron [4] (purple) and gold [5] (gray). The pressure-temperature space that can be typically explored with laser (LH) or resistive (RH) heated diamond anvil cells (DACs) is shown as a gray shaded area. The Hugoniot (dashed lines) and isentrope (dash-dotted lines) curves for Fe and Au represent typical conditions obtained upon shock and ramp compression. Pink and cyan shaded areas qualitatively represent the warm dense matter (WDM) and the *cold* HED matter regimes to give an idea of how they can be accessed with high-pressure and high-temperature experiments. The picture of the Earth is centered on our planet's core conditions.

*Contact author: coppari1@llnl.gov

Published by the American Physical Society under the terms of the Creative Commons Attribution 4.0 International license. Further distribution of this work must maintain attribution to the author(s) and the published article's title, journal citation, and DOI.

corresponding to 10^{11} J/m^3 for representative materials (solid lines) in temperature-pressure space. Comparing the curves corresponding to deuterium (navy), iron (purple), and gold (gray) shows how the energy density depends not only on pressure and temperature but also on material properties. Lower atomic-number and more compressible materials reach 10^{11} J/m^3 at lower pressures, and the pressure required to attain this energy-density threshold decreases at higher temperature. For instance, deuterium has an energy density of 10^{11} J/m^3 at 200 GPa at room temperature and at 100 GPa at 5000 K, whereas iron must be compressed to almost 500 GPa at ambient temperature and to about 300 GPa at 10 000 K to cross this threshold. Does this imply that iron at 300 GPa and 6000 K, roughly corresponding to the Earth's core conditions, is not in a HED state? Probably not. In fact, as I will present in this Essay, my perspective on HED science is more focused on the materials' behavior, rather than anchored solely in an HED value.

Collective behavior in HED matter—A defining feature of HED materials is that collective effects dominate their behavior. HED matter can exist in the solid, liquid, or plasma states, provided its density is high enough for these collective effects to be important.

At extremely high temperatures, on the order of hundreds of eV or higher (1 eV $\approx 10^4$ K, off the scale in Fig. 1), matter exists in a plasma state. Classical plasmas are typically characterized by densities well below 1 g/cm^3 and are usually treated as ionized gases of isolated ions and electrons. In HED plasmas or *dense plasmas*, however, the density can exceed solid-state values and particle correlations become important. Moreover, whereas the pressure in a classical plasma is essentially thermal, Coulomb interactions become significant in the dense plasma regime. This behavior is illustrated by the coupling parameter $\Gamma = (Ze)^2/r_0 kT$, where Z is the ion charge state, e is the electron charge, r_0 is the average distance between ions, k is the Boltzmann constant, and T is the ion temperature [6]. Γ is the ratio between the interatomic potential energy and the thermal energy. For a classical plasma, $\Gamma \ll 1$, while it approaches unity as the density increases, signaling the onset of the HED regime. Dense plasmas are found in stellar interiors, including in the core of the Sun, where temperatures and densities are so high that fusion occurs [7], but also in giant planet interiors such as Jupiter and Saturn, where matter can exist as dense ionized or partially ionized plasmas. In the laboratory, dense plasmas are generated in inertial and magnetic confinement fusion experiments [8], in strong laser-matter interactions, and also in shock-compressed matter generated by lasers, gas guns or pulsed power machines [6].

At temperatures of a few eV, materials enter the warm dense matter regime (pink shaded area in Fig. 1). In this complex state of matter [9,10], $\Gamma \gtrsim 1$, typical pressures reach hundreds of GPa, and densities are comparable to or greater than those of solids. Electron degeneracy, partial ionization, and quantum effects all play crucial roles in determining the properties of WDM. Warm dense matter occurs naturally in planetary and brown dwarf interiors, as well as in the outer layers of white dwarf stars [11]. It is also generated in the laboratory when solids are shocked or isochorically heated [12], and also by interactions with x-ray free electron lasers (XFELs).

At lower temperatures (below a few thousand kelvin), matter exists in condensed solid or liquid states (cyan-shaded area in Fig. 1). When solids or liquids are squeezed to sufficiently high pressure, they also enter the HED regime, forming what I will refer to throughout as *cold* HED matter. Here, atoms are forced so close to each other that Coulomb interactions become important and bound-electron wave functions begin to overlap. In HED solids, $\Gamma \gtrsim 100$, densities far exceed ambient solid densities, and the interplay of compression and heating induces new material properties. As interatomic spacings decrease, quantum effects increasingly govern material behavior, and overlapping electronic bands fundamentally alter transport, chemical, and mechanical properties. Structural and electronic phase transformations may occur, inducing further dramatic changes in the physicochemical behavior. Cold HED matter is found in the interiors of large terrestrial planets [13] and can also be generated in the laboratory as I will discuss in this Essay.

Despite the ubiquity of HED conditions across states of matter, HED science has historically been tied to plasma physics, likely because it originated in nuclear fusion research and astrophysics, both firmly rooted in plasma science. Recent technical developments, however, made the generation of cold HED matter (also referred to as *quantum matter* [14]), more readily achievable in the laboratory, giving increased emphasis to this rather unexplored HED regime which arises at relatively low temperatures and very high pressures. This evolution raises fundamental questions for the field: how are the different HED regimes connected? Through what mechanisms do materials transform from one regime to another? What new physics emerges at the interface of plasma physics, warm dense matter, and *cold* HED matter?

Experimental generation and characterization of cold HED matter—Producing cold HED matter in the laboratory requires reaching extreme pressure while keeping the temperature relatively low. This has become feasible thanks to recent developments of new experimental capabilities, notably the laser-driven ramp-compression technique combined with *in situ* x-ray diffraction, and improved diamond anvil cell (DAC) technology with high-temperature capabilities (Fig. 2). These experimental tools will let us probe fundamental questions about solids at extreme conditions: how does a solid behave when pressure shrinks interatomic distances to the scale of the electron de Broglie wavelength? How does the competing effect of pressure (which

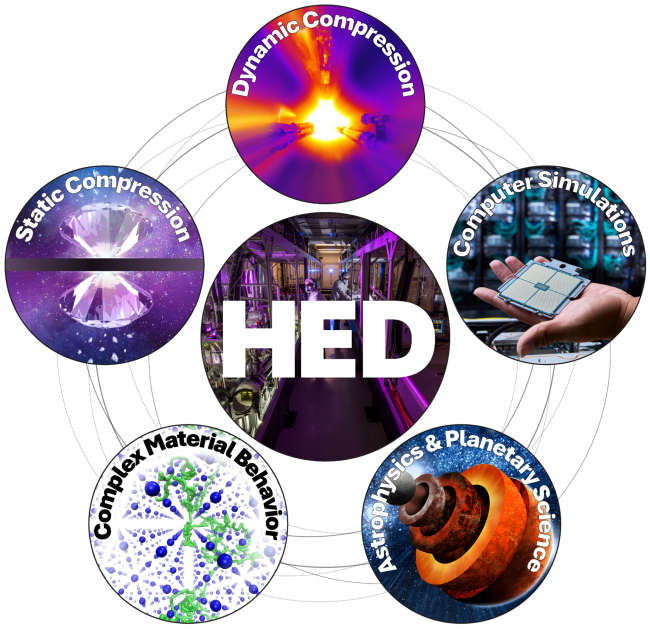


FIG. 2. HED science is a rich research field where experiments at extreme conditions, using both static and dynamic compression, and state-of-the art computational methods reveal the complex behavior of HED matter (shown here is a snapshot from density functional theory simulations of the superionic water ice structure) and its application for astrophysics and planetary science. Figure credit: B. Chavez/LLNL. Visual for complex material behavior credit: S. Hamel/LLNL.

squeezes atoms together) and temperature (which drives thermal motion) affect materials' properties? More broadly, what does *matter* mean under these extreme conditions?

In laser-driven dynamic compression, high-intensity lasers ablate a solid surface, creating an expanding plasma that, by momentum conservation, drives compression waves back into the material. If these waves exceed the material's sound speed, they steepen into a shock, a sharp jump in pressure, density, and temperature governed by the Rankine-Hugoniot relations [15,16]. Shock compression induces high-pressure states but also causes strong heating, often melting the material at relatively modest pressures and readily producing WDM or dense plasmas. Ramp (or quasi-isentropic) compression instead applies a sequence of weaker compression waves over longer timescales (tens of nanoseconds), [17] reducing entropy generation and keeping the temperature much closer to the isentrope (pressure-temperature conditions reached upon compression at constant entropy [18]) than to the Hugoniot of the material (conditions obtained upon propagation of a single shock). Ramp compression is therefore ideal to generate cold HED matter, achieving extreme pressures while maintaining materials in the solid or liquid state (Fig. 1). Combining laser-driven compression with *in situ* x-ray diffraction measurements [19–25], has already provided key insights into the atomic structure, phase transitions, and density of cold HED solids.

Cold HED matter can also be generated using diamond anvil cells combined with heating mechanisms. Developed in the late 1950s, DACs have been the cornerstone of experimental high-pressure condensed matter science [26] and foundational to its development. They produce static high pressures by forcing two opposing diamond anvils together and compressing the sample enclosed between them. Continuous developments pushed the boundaries of attainable pressure to the theoretical pressure limit imposed by the diamond's yield strength of about 400 GPa [27,28]. New designs, such as double-stage [29,30] and toroidally shaped [31,32] anvils, now exceed this limit, reaching a static pressure of 1 TPa at room temperature [30]. Coupling DACs with resistive or laser heating [33,34]) expands the region of the phase diagram obtainable with static compression beyond room temperature, although reducing the maximum pressure. DACs can thus reach pressures of several hundreds GPa at room temperature, and a few hundred GPa and a few thousand degrees kelvin when combined with laser-heating mechanisms, making them a complementary platform for recreating HED conditions (see gray shaded area in Fig. 1), and specifically cold HED matter.

X-ray free electron lasers are another rapidly emerging technology central to future developments of HED science. XFELs are large-scale light sources that generate coherent, ultrabright, femtosecond x-ray pulses, with tunable energy and MHz repetition rate [35–37], enabling time-resolved measurements of atomic-scale structures and electronic states with unprecedented spatial and temporal resolution. In the cold HED regime, such rapid atomic- and electronic-level changes can be induced by shock or ramp compression [38,39], or by dynamic DAC—that is, DAC equipped with a piezoelectric actuator that enables compression on timescales as fast as milliseconds [40]. Dedicated beamlines that combine hundreds of joules lasers or DAC devices with XFEL radiation are already operational in major XFEL facilities, such as the Matter at Extreme Conditions (MEC) station at the Linac Coherent Light Source (LCLS) [41] and the HED Instrument at the European XFEL (EuXFEL) [42]. These capabilities will enable detailed investigations of how phase transitions and kinetic effects depend on strain rate, including nonequilibrium phenomena.

Superionic water ices at HED conditions—A remarkable discovery enabled by these new technologies is the existence of superionic water ice first predicted in the late 1980s [43,44]. In a superionic phase, one atomic species, typically the heavier element, forms a solid lattice, while the lighter element diffuses through it like a liquid. Computational studies have explored the pressures and temperatures required for the onset of the superionic ice regime, along with its structural, transport, and thermodynamic properties [45–48]. Because water must be

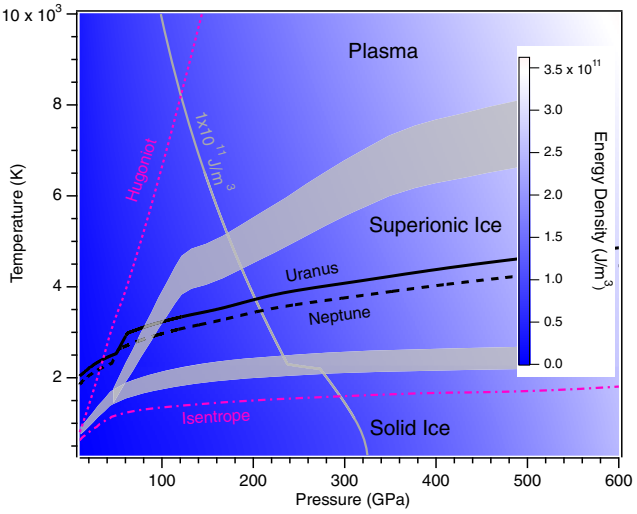


FIG. 3. Temperature-pressure diagram of water. The color background represents the energy density in J/m^3 (color scale on the right) calculated from the AQUA tabular EOS [51]. The 1×10^{11} J/m^3 contour is shown as a gray line. The Hugoniot and principal isentrope of liquid water are shown as pink dotted and dash-dotted lines, respectively [51]. The boundaries for the predicted formation of the superionic ice phase are shown by thick gray bands [52]. Interior temperature-pressure conditions for Uranus and Neptune are shown as the black continuous and dashed lines [53].

compressed to high pressures and temperatures (Fig. 3) to become superionic, and because *in situ* diagnostics are difficult at these conditions, experimental validation did not occur until much later in laser-driven compression experiments [49,50].

Dynamically compressing water into the superionic regime is particularly challenging because neither pure shock compression nor pure ramp compression can reach the necessary conditions (Hugoniot and isentrope curves in Fig. 3). Instead, a precise combination of a weak initial shock to ∼15 to ∼70 GPa followed by a ramp pulse is required to reach high-pressure states between 2000 and 4000 K, where the superionic phase is predicted to form. A precisely timed x-ray burst is then needed to capture the atomic structure of the compressed water [50]. More recently, experiments using DAC combined with resistive and laser heating have not only reproduced these findings, but also revealed polymorphism within the superionic phase, [54–56] further underscoring the complexity of HED matter (Fig. 2).

The challenge associated with the detection of superionic phases relates to the fact that it is extremely hard to measure the diffusing species directly. The x-ray scattering signature would, in fact, resemble that observed in liquids, where the absence of long-range periodic order gives rise to broad diffuse maxima, or "halos," arising from short-range atomic correlations. Such a signal is typically very weak and difficult to detect under high-pressure, high-temperature conditions. In the experiments discussed here, the superionic nature of the ice was inferred from optical conductivity measurements [49,55] and/or from thermodynamic arguments [50,54,55]. The brightness of XFEL-generated x-rays has already enabled the detection of the liquid signal in shock-compressed materials [57,58]. Looking ahead, it could also allow measurements of the liquid-like scattering signature originating from the diffusing hydrogens.

Kinetic effects and compression at high strain rate—What are the relevant timescales for equilibrium phase transitions? Can high-strain-rate compression truly produce equilibrium in matter at extreme conditions? These remain open questions in HED physics. While thermodynamics tells us what the equilibrium phase transition should be, kinetics determines how, and how quickly, it occurs. When pressure and temperature change faster than the characteristic time required for equilibrium transformations, kinetic effects may dominate whether a transition happens and what phase emerges.

While dynamic compression drives materials to extreme states on nanosecond to microsecond timescales [59,60], DACs can sustain pressure for seconds or even minutes, providing access to equilibrium or close-to-equilibrium properties. Taken together, dynamic and static compression span a broad strain-rate range (from $\sim 10^9$ s^{-1} to 10^{-3} s^{-1}), enabling systematic investigation of strain-rate effects on phase transitions, and elucidating the role of kinetics in the material's response. Varying the probe duration may also bring new phenomena into light. At large laser facilities, materials are compressed on nanosecond timescales and typically probed with nanosecond x-ray flashes [61]. Using laser drivers on synchrotrons and XFELs beamlines maintains the nanosecond compression times, allowing much shorter probes, from picosecond x-ray pulses [62] down to femtosecond-long probes [41,42,63]. Despite these capabilities, there is still a lot to understand about the response of materials to high-strain-rate compression and phase transition kinetics. Do materials follow common trends governed by their electronic or crystal structure? Or is the response strongly material specific, i.e., dependent on the atomic species?

For tantalum, for example, melting has been observed at the same conditions across a broad timescale, from a few seconds in laser-heated DAC experiments [64] down to the microseconds [65] and nanoseconds [66] in shock compression generated by gas gun and lasers, suggesting that equilibrium conditions are reached. Diamond, instead, provides a contrasting example. Experiments using nanosecond compression and probe times [67] suggest that kinetic barriers may hinder the transformation to the theoretically predicted stable phases on such timescales. Diamond, the metastable form of carbon recoverable at ambient conditions, is characterized by a strong sp^3 bond responsible for the persistence of this structure to very high pressures. Theory predicts that this metastability should

break down in the TPa regime: density functional theory (DFT) and *ab initio* random search calculations have identified a different tetrahedrally coordinated cubic structure than diamond (called BC8) to become stable above 1 TPa and a simple cubic structure to be stable above 3 TPa [68–70]. Yet, laser-driven ramp-compression experiments reaching 2 TPa, combined with *in situ* x-ray diffraction, have found no evidence for the formation of BC8 carbon [67], possibly due to the high energy barrier (estimated to be ∼2.5 eV/atom [71]) to overcome to form the thermodynamically stable structure. Recent quantum-accurate multimillion-atom molecular dynamics simulations confirm that the BC8 structure is only accessible in a narrow pressure-temperature region of the carbon phase diagram, where temperature is sufficiently high to induce significant atomic mobility and where the melting initiating at the grain boundary seeds the BC8 transformation [72]. Integrating experiments spanning many orders of magnitude in timescales with state-of-the-art simulations will be essential for unraveling such complex phase-transition pathways (Fig. 2).

XFELs have also been used to study kinetic effects in HED materials. Examples include the investigation of superionic ice formation kinetics at a few tens of GPa and high temperature, induced by pulsed, femtosecond x-ray heating [73], and the formation of metastable ice structures along complex crystallization pathways [74]. These works show that material structure and phase boundaries can be strongly path dependent and that metastable phases can exert significant control over crystallization. Although the pressures currently achievable at XFEL facilities are relatively modest, future developments on the pressure generation front (more energetic laser drivers for example) should enable the investigation of the pathway dependence of phase transitions happening at more extreme conditions.

The complexity of cold HED matter—As tools for generating and characterizing matter at extreme conditions advance, a pattern emerges: solids seem to become more complex as pressure and temperature conditions become more extreme (Fig. 2). A fascinating example of the extreme complexity of HED solids is the formation of *high-pressure electride phases*.

Electrides are materials in which electrons localize in the interstitial regions of the lattice, rather than being around the nuclei or forming bonds. Their discovery at high pressure provides a vivid example of unexpected material behavior at extreme conditions and challenges the common expectation that compression drives materials toward close-packed metals. This expectation is grounded in the observation that, as atoms are squeezed together, their atomic orbitals are smeared out, allowing outer electrons to delocalize, turning matter into metals.

However, experiments and simulations at HED conditions reveal a more complex picture: pressure can also turn metals into insulators. Sodium, long regarded as a prototypical example of *simple* free-electron metal, was first predicted [75] and later observed to become an insulator in room temperature high-pressure DAC experiments near 200 GPa [76,77]. The metal-to-insulator transition arises because pressure induces significant overlap of core electrons, eventually making it more energetically favorable for the system to force the electron clouds into interstitial sites, forming a high-pressure electride phase [75,78]. This electronic reorganization is often accompanied by a structural transition to a more open structure than the lower-pressure phase, contributing to the counterintuitive nature of materials at extreme conditions [79,80]. This behavior, first predicted in simple metals, most notably Na and Li [81,82], is now expected (and in some cases indirectly observed) also in other systems, such as Al [79], Mg [80,83], carbon [70], and compounds [84]. These results raise important open questions: is the formation of electride phases ubiquitous at high pressure? Do all materials eventually become electrides at sufficiently high pressure? More research is needed to answer this question. Interestingly, computational work suggests that electride-like behavior may also occur in liquids, highlighting how this phenomenon may be more common than initially thought [85,86]. Experimentally, however, determining if a solid is in fact an electride is a challenging task. Often, the signature in x-ray diffraction measurements is a subtle change in the diffraction peak intensity, which is extremely difficult to quantify with high precision. The brightness of XFEL-generated x-ray sources offers a possible route to more direct measurements. Currently, however, driver lasers at XFEL facilities are limited to ∼100 J of energy, preventing access to the pressures at which materials are predicted to become electrides. Future upgrades of these laser systems may overcome this limitation and enable systematic experimental studies of high-pressure electride phases.

HED matter and the interior structure of planets—A fascinating manifestation of HED matter occurs in planetary interiors (Fig. 2). Depending on the planet's size and composition, its constituent materials might assume different HED states. In gas giant planets such as Jupiter and Saturn, hydrogen and helium—which account for most of their mass—are expected to exist in a dense plasma regime at the extreme interior conditions that may reach values as high as 4 TPa and 20 000 K in Jupiter's deep core [87]. In contrast, terrestrial planets consist primarily of heavier elements and compounds, including silicates, oxides, and iron-based minerals and alloys. In these rocky planets, gravity raises the internal pressure enough to keep materials below or near their melting temperatures, even at the thousands of degrees expected in their interiors. As a result, materials inside large terrestrial planets are likely to be in the WDM or in the cold HED matter regime. Understanding the structural and transport properties of the

fundamental building blocks of planets at these relatively cold and compressed HED conditions is essential for accurately modeling their interior structure.

Because at the moment we must rely on limited data from astronomical observations, modeling a planet's internal structure is a complex task. This is especially true for *extrasolar planets*, where available data are often limited to the planet's mass and radius [88]. These data are combined with the equations of state for materials believed to constitute their interiors to build a structural model that matches observations. However, since planets are not made of a single material, and their composition itself is uncertain, there are often many different models that can match the observables [13,89]. Additionally, when experimental data on material properties are unavailable for the planets' interior conditions, a common—although usually misleading—approach is to extrapolate data collected at a different pressure and temperature range. This practice neglects the complex material behavior that emerges under HED conditions and inevitably propagates systematic inaccuracies in the interior-structure models. Performing experiments at planetary HED conditions is therefore critical to help address this problem.

To expand on the example discussed earlier, the formation of a superionic form of ice at specific temperature and pressure conditions may have strong implications for the interior structure of the ice giants, Uranus and Neptune, as well as of extrasolar planets [88]. Figure 3 shows a possible temperature-pressure profile for Uranus and Neptune [53] overlayed on the water phase diagram. At about 100 GPa, the planetary adiabats cross the fluid to superionic phase boundary, suggesting that a parcel of water at a given depth inside the planet might become superionic. This would imply that Uranus and Neptune may not be characterized by a single layer of fluid water, but instead may exhibit stratifications, with implications for the generation of their magnetic field [50,90]. Obviously, water in planetary interiors does not exist in pure form, and it is likely mixed with other species such as methane and ammonia, and possibly even rocks [89]. Numerical calculations suggest that a superionic phase may still form in such a mixed environment [91], although the pressure-temperature conditions at which this occurs may differ from those of pure water, impacting the depth and nature of the planet's layered structure.

Mixing of materials at extreme conditions is another grand challenge of HED science. Do materials that mix at certain conditions demix at higher pressures and temperatures? Intuition suggests that increasing temperature should favor mixing, and that materials that mix at Earth's interior conditions should also mix at the most extreme conditions of larger (exo)planets. However, the complex physicochemical behavior of HED materials may lead to different outcomes. Simulations indicate, for example, that water might become a superacid at the extreme conditions expected inside the ice giant planets. This can trigger hydrocarbon condensation in the presence of methane, which can, in turn, lead to nanodiamond precursors [92], further increasing the complexity of the planet's internal structure. Similarly, experiments on oxides suggest that phase transitions at pressure and temperature exceeding those inside the Earth may dramatically affect their ability to mix, leading to exsolution and miscibility gaps that create complex stratifications inside large terrestrial planets [93,94].

Transport properties of planet-forming materials at HED conditions, such as viscosity, electrical, and thermal conductivities, are also critical for planetary modeling as they regulate the dynamics, magnetic field generation, and heat transfer. Measuring these properties is, however, extremely challenging. Most of the experimental data to date come from DAC experiments and are limited to a few hundred GPa pressure range at high temperature [95,96]. In dynamic compression experiments, the reflectivity of the shock front has been used to infer conductivity at more extreme conditions, although this technique is currently limited to transparent samples (such as silicates) and Hugoniot states [97,98]. Viscosity is another key transport property that is particularly difficult to measure. The falling-sphere method —measuring the velocity of a sphere embedded in a fluid and using the Stokes' law to relate the velocity to the fluid viscosity—is probably the most direct approach to obtaining fluid viscosity at high pressure, but current implementations are limited to pressures of only a few GPa [99]. New experimental platforms are being developed to measure viscosity at higher pressure, including under dynamic compression [100]. Advancing these techniques is a key future direction for HED science and will significantly improve our understanding of material properties at extreme conditions and their applications for planetary interior structure modeling.

Artificial intelligence and machine learning applications in HED physics—Unprecedented opportunities for progress in every scientific field, including HED science, are emerging with the application of artificial intelligence (AI) tools. HED physics is entering a data-driven era, in which machine learning (ML), Bayesian inference, and surrogate modeling are becoming essential for understanding, designing, and operating highly nonlinear, multiphysics experiments [101]. In the HED field, AI methods are already being used to support complex data analysis [102], aid experimental operations at large user laser facilities [103], and to advance DFT-based simulations of material properties [104,105]. ML algorithms are capable of combining large heterogeneous datasets, improving predictive fidelity and computational costs. Rising shot rates, such as those existing at XFEL and other high repetition rate facilities, together with growing datasets, demand automated, algorithm-based workflows for experiment control, real-time analysis, and model updating. The use of AI has

the potential to dramatically accelerate discovery by enabling fast analysis of massive datasets or even by autonomously executing experiments, where robotics and self-driving laboratories will reduce downtime while ensuring tracking and quality control at a pace that would be unthinkable for human standards.

There are still significant challenges associated with the use of AI in physics in general, largely related to data scarcity for AI training purposes, physics fidelity, uncertainty quantification, and the need for rigorous validation [106]. The community will have to address these issues to ensure a reliable and ethical deployment of AI tools and to steer the paradigm shift that the AI revolution represents in a beneficial direction.

Concluding remarks—HED science investigates regimes where energy densities match or exceed interatomic or electronic binding energies, driving strong coupling, substantial ionization, and leading to transitions to unexpected states. Encompassing plasma, warm dense matter, and condensed matter physics, HED research naturally bridges disciplinary boundaries and unites different scientific communities. Emerging experimental platforms, continuous refinement of more established techniques, and fast-growing AI and ML tools now enable unprecedented studies of matter under more and more extreme conditions, accessing entirely new regimes of physics. The growing emphasis on cold HED matter, formed at extreme pressures and relatively low temperatures, illustrates how technological advances enable scientists to push the boundaries of experimental discovery. The direct observations and quantification of previously inaccessible phenomena reveal the rich and complex behavior of this emerging HED regime, including transitions to novel states of matter such as superionic and electride phases, as well as metastability and path-dependent material responses under ultrahigh pressures, temperatures and compression rates. HED science is a rapidly advancing field posing fundamental questions and underpinning a wide range of applications, from astrophysics and planetary science to fusion energy. Together, these features underscore the tremendous potential and critical need to foster a vibrant, interdisciplinary HED science community. Closer collaborations among planetary scientists, condensed matter and plasma physicists, and fusion researchers will keep driving groundbreaking discoveries, anchored by a shared scientific vision and cutting-edge technology.

Acknowledgments—I gratefully acknowledge William (Will) Evans for mentorship and influential contributions to the field. I am indebted to many colleagues for discussions and/or feedback on the manuscript, including Heather Whitley, Bruce Remington, Marius Millot, Madison Martin, Michael MacDonald, Peter Celliers, David Bradley, Jon Eggert, and Philip Sterne. This work was performed under the auspices of the U.S. Department of Energy by Lawrence Livermore National Laboratory under Contract No. DE-AC52-07NA27344.

Data availability—No data were created or analyzed in this study.



. **Federica Coppari**

Federica Coppari is a research scientist at Lawrence Livermore National Laboratory (LLNL), where she serves on the leadership team of the High Energy Density Science Center. Dr. Coppari manages the LLNL/University of California collaboration in HEDS and oversees the Consortium for High Energy Density Science, a research partnership between LLNL and U.S. academic institutions. She received her B.S. and M.S. degrees in Physics from the University of Camerino, Italy, and her Ph.D. in Materials Science from Pierre and Marie Curie University, France, in 2010. Her work focuses on experimentally investigating material properties under extreme pressure and temperature conditions, with particular emphasis on phase transitions and equations of state. Dr. Coppari was named a New Leader for Space Science by the U.S. National Academy of Sciences and the Chinese Academy of Sciences in 2019, and in 2020, she received the Department of Energy Early Career Research Program Award from the Office of Fusion Energy Sciences.

[1] R. Drake, *High-Energy-Density Physics: Fundamentals, Inertial Fusion, and Experimental Astrophysics*, Shock Wave and High Pressure Phenomena (Springer, Berlin Heidelberg, 2006).

[2] J. Larsen, *Foundations of High-Energy-Density Physics: Physical Processes of Matter at Extreme Conditions* (Cambridge University Press, Cambridge, England, 2017).

[3] D. Saumon, The sesame 5267 equation of state of deuterium, Technical Report, LA-UR-13-20032, Los Alamos National Laboratory.

[4] C. J. Wu *et al.*, Wide-ranged multiphase equation of state for iron and model variations addressing uncertainties in high-pressure melting, Phys. Rev. B **108**, 014102 (2023).

[5] G. I. Kerley, Equations of state for Be, Ni, W, and Au, Technical Report, SAND 2003-3784, Sandia National Laboratories (2003).

[6] J. Colvin and J. Larsen, *Extreme Physics* (Cambridge University Press, Cambridge, England, 2013).

[7] D. T. Casey *et al.*, Thermonuclear reactions probed at stellar-core conditions with laser-based inertial-confinement fusion, Nat. Phys. **13**, 1227 (2017).

[8] O. A. Hurricane, P. K. Patel, R. Betti, D. H. Froula, S. P. Regan, S. A. Slutz, M. R. Gomez, and M. A. Sweeney, Physics principles of inertial confinement fusion and U.S. program overview, Rev. Mod. Phys. **95**, 025005 (2023).

[9] D. Riley, Generation and characterisation of warm dense matter with intense lasers, Plasma Phys. Controlled Fusion **60**, 014033 (2018).

[10] J. Vorberger *et al.*, Roadmap for warm dense matter physics, Plasma Phys. Controlled Fusion **68**, 073501 (2026).

[11] D. Saumon, S. Blouin, and Tremblay, P.-E. Current challenges in the physics of white dwarf stars, Phys. Rep. **988**, 1 (2022).

[12] M. Bailly-Grandvaux *et al.*, Creation and characterization of warm dense matter isochorically heated by an intense laser-driven proton beam to temperatures exceeding 100 eV, Commun. Phys. **8**, 285 (2025).

[13] A. Boujibar, P. Driscoll, and Y. Fei, Super-Earth internal structures and initial thermal states, J. Geophys. Res. **125**, e2019JE006124 (2020).

[14] *Fundamental Research in High Energy Density Science* (The National Academies Press, Washington, DC, 2023).

[15] Y. Zel'dovich and Y. P. Raizer, *Physics of Shock Waves and High-Temperature Hydrodynamic Phenomena* (Academic Press Inc., New York, 1966).

[16] L. Davison and R. Graham, Shock compression of solids, Phys. Rep. **55**, 255 (1979).

[17] D. C. Swift and R. P. Johnson, Quasi-isentropic compression by ablative laser loading: Response of materials to dynamic loading on nanosecond time scales, Phys. Rev. E **71**, 066401 (2005).

[18] It is important to point out that ramp compression of materials results in temperatures that are somewhat higher than the material's isentrope. This is because the plastic work performed by the uniaxial compression at high strain rate is dissipated as heat [J. Mason, A. Rosakis, and G. Ravichandran, On the strain and strain rate dependence of the fraction of plastic work converted to heat: An experimental study using high speed infrared detectors and the Kolsky bar, Mech. Mater. **17**, 135 (1994)].

[19] J. S. Wark, R. R. Whitlock, A. A. Hauer, J. E. Swain, and P. J. Solone, Subnanosecond x-ray diffraction from laser-shocked crystals, Phys. Rev. B **40**, 5705 (1989).

[20] D. H. Kalantar *et al.*, Multiple film plane diagnostic for shocked lattice measurements (invited), Rev. Sci. Instrum. **74**, 1929 (2003).

[21] J. R. Rygg *et al.*, Powder diffraction from solids in the terapascal regime, Rev. Sci. Instrum. **83**, 113904 (2012).

[22] J. M. Foster *et al.*, X-ray diffraction measurements of plasticity in shock-compressed vanadium in the region of 10–70 GPa, J. Appl. Phys. **122**, 025117 (2017).

[23] J. R. Rygg *et al.*, X-ray diffraction at the National Ignition Facility, Rev. Sci. Instrum. **91**, 043902 (2020).

[24] A. Denoeud *et al.*, X-ray powder diffraction in reflection geometry on multi-beam kJ-type laser facilities, Rev. Sci. Instrum. **92**, 013902 (2021).

[25] T. Xi *et al.*, Real-time x-ray diffraction measurement on laser shock-loaded hexanitrostilbene (HNS), Energetic Mater. Front. **5**, 224 (2024).

[26] W. A. Bassett, Diamond anvil cell, 50th birthday, High Press. Res. **29**, 163 (2009).

[27] M. I. Eremets, I. A. Trojan, P. Gwaze, J. Huth, R. Boehler, and V. D. Blank, The strength of diamond, Appl. Phys. Lett. **87**, 141902 (2005).

[28] I. O'Bannon, F. Earl, Z. Jenei, H. Cynn, M. J. Lipp, and J. R. Jeffries, Contributed review: Culet diameter and the achievable pressure of a diamond anvil cell: Implications for the upper pressure limit of a diamond anvil cell, Rev. Sci. Instrum. **89**, 111501 (2018).

[29] L. Dubrovinsky, N. Dubrovinskaia, V. B. Prakapenka, and A. M. Abakumov, Implementation of micro-ball nanodiamond anvils for high-pressure studies above 6 Mbar, Nat. Commun. **3**, 1163 (2012).

[30] N. Dubrovinskaia *et al.*, Terapascal static pressure generation with ultrahigh yield strength nanodiamond, Sci. Adv. **2**, e1600341 (2016).

[31] A. Dewaele, P. Loubeyre, F. Occelli, O. Marie, and M. Mezouar, Toroidal diamond anvil cell for detailed measurements under extreme static pressures, Nat. Commun. **9**, 2913 (2018).

[32] Z. Jenei, E. F. O'Bannon, S. T. Weir, H. Cynn, M. J. Lipp, and W. J. Evans, Single crystal toroidal diamond anvils for high pressure experiments beyond 5 megabar, Nat. Commun. **9**, 3563 (2018).

[33] S. Pasternak, G. Aquilanti, S. Pascarelli, R. Poloni, B. Canny, M.-V. Coulet, and L. Zhang, A diamond anvil cell with resistive heating for high pressure and high temperature x-ray diffraction and absorption studies, Rev. Sci. Instrum. **79**, 085103 (2008).

[34] A. F. Goncharov, J. A. Montoya, N. Subramanian, V. V. Struzhkin, A. Kolesnikov, M. Somayazulu, and R. J. Hemley, Laser heating in diamond anvil cells: Developments in pulsed and continuous techniques, J. Synchrotron Radiat. **16**, 769 (2009).

[35] T. Ishikawa *et al.*, A compact x-ray free-electron laser emitting in the sub-ångström region, Nat. Photonics **6**, 540 (2012).

[36] J. Park *et al.*, Design of a hard x-ray beamline and end-station for pump and probe experiments at Pohang

Accelerator Laboratory X-ray Free Electron Laser facility, Nucl. Instrum. Methods Phys. Res., Sect. A **810**, 74 (2016).
[37] W. Decking *et al.*, A MHz-repetition-rate hard x-ray free-electron laser driven by a superconducting linear accelerator, Nat. Photonics **14**, 391 (2020).
[38] D. Milathianaki *et al.*, Femtosecond visualization of lattice dynamics in shock-compressed matter, Science **342**, 220 (2013).
[39] J. S. Wark, M. I. McMahon, and J. H. Eggert, Femtosecond diffraction and dynamic high pressure science, J. Appl. Phys. **132**, 080902 (2022).
[40] W. J. Evans, C.-S. Yoo, G. W. Lee, H. Cynn, M. J. Lipp, and K. Visbeck, Dynamic diamond anvil cell (dDAC): A novel device for studying the dynamic-pressure properties of materials, Rev. Sci. Instrum. **78**, 073904 (2007).
[41] B. Nagler *et al.*, The matter in extreme conditions instrument at the linac coherent light source, J. Synchrotron Radiat. **22**, 520 (2015).
[42] U. Zastrau *et al.*, The high energy density scientific instrument at the European XFEL, J. Synchrotron Radiat. **28**, 1393 (2021).
[43] P. Demontis, R. LeSar, and M. L. Klein, New high-pressure phases of ice, Phys. Rev. Lett. **60**, 2284 (1988).
[44] C. Cavazzoni, Superionic and metallic states of water and ammonia at giant planet conditions, Science **283**, 44 (1999).
[45] M. French and R. Redmer, Optical properties of water at high temperature, Phys. Plasmas **18**, 043301 (2011).
[46] M. French, M. P. Desjarlais, and R. Redmer, *Ab initio* calculation of thermodynamic potentials and entropies for superionic water, Phys. Rev. E **93**, 022140 (2016).
[47] H. F. Wilson, M. L. Wong, and B. Militzer, Superionic to Superionic Phase change in water: Consequences for the interiors of uranus and neptune, Phys. Rev. Lett. **110**, 151102 (2013).
[48] J. A. Hernandez and R. Caracas, Superionic-superionic phase transitions in body-centered cubic H2 O Ice, Phys. Rev. Lett. **117**, 135503 (2016).
[49] M. Millot, S. Hamel, J. R. Rygg, P. M. Celliers, G. W. Collins, F. Coppari, D. E. Fratanduono, R. Jeanloz, D. C. Swift, and J. H. Eggert, Experimental evidence for superionic water ice using shock compression, Nat. Phys. **14**, 297 (2018).
[50] M. Millot, F. Coppari, J. R. Rygg, A. C. Barrios, S. Hamel, D. C. Swift, and J. H. Eggert, Nanosecond x-ray diffraction of shock-compressed superionic water ice, Nature (London) **569**, 251 (2019).
[51] J. Haldemann, Y. Alibert, C. Mordasini, and W. Benz, AQUA: A collection of H_2O equations of state for planetary models, Astron. Astrophys. **643**, A105 (2020).
[52] R. Redmer, T. R. Mattsson, N. Nettelmann, and M. French, The phase diagram of water and the magnetic fields of Uranus and Neptune, Icarus **211**, 798 (2011).
[53] B. Militzer, *Ab initio* entropy calculations of water predict the interiors of uranus and neptune to be 15%–30% colder than previous models, Astrophys. J. **990**, 20 (2025).
[54] J. A. Queyroux *et al.*, Melting curve and isostructural solid transition in superionic ice, Phys. Rev. Lett. **125**, 195501 (2020).
[55] V. B. Prakapenka, N. Holtgrewe, S. S. Lobanov, and A. F. Goncharov, Structure and properties of two superionic ice phases, Nat. Phys. **17**, 1233 (2021).
[56] G. Weck, J.-A. Queyroux, S. Ninet, F. Datchi, M. Mezouar, and P. Loubeyre, Evidence and stability field of fcc superionic water ice using static compression, Phys. Rev. Lett. **128**, 165701 (2022).
[57] M. Gorman *et al.*, Shock compression experiments using the DiPOLE 100-X laser on the high energy density instrument at the European x-ray free electron laser: Quantitative structural analysis of liquid Sn, J. Appl. Phys. **135**, 165902 (2022).
[58] G. Morard *et al.*, Structural evolution of liquid silicates under conditions in Super-Earth interiors, Nat. Commun. **15**, 8483 (2024).
[59] H. F. Swift, *Light-Gas Gun Technology: A Historical Perspective* (Springer, Berlin, Heidelberg, 2005), pp. 1–35.
[60] W. A. Stygar, M. E. Cuneo, D. I. Headley, H. C. Ives, R. J. Leeper, M. G. Mazarakis, C. L. Olson, J. L. Porter, T. C. Wagoner, and J. R. Woodworth, Architecture of petawatt-class *z*-pinch accelerators, Phys. Rev. ST Accel. Beams **10**, 030401 (2007).
[61] F. Coppari, R. F. Smith, D. B. Thorn, J. R. Rygg, D. A. Liedahl, R. G. Kraus, A. Lazicki, M. Millot, and J. H. Eggert, Optimized x-ray sources for x-ray diffraction measurements at the Omega Laser Facility, Rev. Sci. Instrum. **90**, 125113 (2019).
[62] D. Broege *et al.*, The Dynamic Compression Sector laser: A 100-J UV laser for dynamic compression research, Rev. Sci. Instrum. **90**, 053001 (2019).
[63] K. Tono *et al.*, Beamline, experimental stations and photon beam diagnostics for the hard x-ray free electron laser of SACLA, New J. Phys. **15**, 083035 (2013).
[64] A. Dewaele, M. Mezouar, N. Guignot, and P. Loubeyre, High melting points of tantalum in a laser-heated diamond anvil cell, Phys. Rev. Lett. **104**, 255701 (2010).
[65] M. C. Akin, J. H. Nguyen, M. A. Beckwith, R. Chau, W. P. Ambrose, O. V. Fat'yanov, P. D. Asimow, and N. C. Holmes, Tantalum sound velocity under shock compression, J. Appl. Phys. **125**, 145903 (2019).
[66] R. G. Kraus, F. Coppari, D. E. Fratanduono, R. F. Smith, A. Lazicki, C. Wehrenberg, J. H. Eggert, J. R. Rygg, and G. W. Collins, Melting of tantalum at multimegabar pressures on the nanosecond timescale, Phys. Rev. Lett. **126**, 255701 (2021).
[67] A. Lazicki *et al.*, Metastability of diamond ramp-compressed to 2 TPa, Nature (London) **589**, 532 (2021).
[68] M. T. Yin, Si-III (BC-8) crystal phase of Si and C: Structural properties, phase stabilities, and phase transitions, Phys. Rev. B **30**, 1773 (1984).
[69] A. A. Correa, S. A. Bonev, and G. Galli, Carbon under extreme conditions: Phase boundaries and electronic properties from first-principles theory, Proc. Natl. Acad. Sci. U.S.A. **103**, 1204 (2006).
[70] M. Martinez-Canales, C. J. Pickard, and R. J. Needs, Thermodynamically stable phases of carbon at multiterapascal pressures, Phys. Rev. Lett. **108**, 045704 (2012).
[71] J. Sun, D. D. Klug, and Martoňák, R. Structural transformations in carbon under extreme pressure: Beyond diamond, J. Chem. Phys. **130**, 194512 (2009).

[72] K. Nguyen-Cong *et al.*, Extreme metastability of diamond and its transformation to the BC8 post-diamond phase of carbon, J. Phys. Chem. Lett. **15**, 1152 (2024).
[73] R. J. Husband *et al.*, Phase transition kinetics of superionic H_2O ice phases revealed by Megahertz x-ray free-electron laser-heating experiments, Nat. Commun. **15**, 8256 (2024).
[74] Y.-H. Lee *et al.*, Multiple freezing–melting pathways of high-density ice through ice XXI phase at room temperature, Nat. Mater. **25**, 302 (2025).
[75] J. B. Neaton and N. W. Ashcroft, On the constitution of sodium at higher densities, Phys. Rev. Lett. **86**, 2830 (2001).
[76] Y. Ma, M. Eremets, A. R. Oganov, Y. Xie, I. Trojan, S. Medvedev, A. O. Lyakhov, M. Valle, and V. Prakapenka, Transparent dense sodium, Nature (London) **458**, 182 (2009).
[77] C. V. Storm *et al.*, Experimental signatures of interstitial electron density in transparent dense sodium, Commun. Mater. **6**, 201 (2025).
[78] M.-S. Miao and R. Hoffmann, High pressure electrides: A predictive chemical and physical theory, Acc. Chem. Res. **47**, 1311 (2014).
[79] C. J. Pickard and R. J. Needs, Aluminium at terapascal pressures, Nat. Mater. **9**, 624 (2010).
[80] M. G. Gorman *et al.*, Experimental observation of open structures in elemental magnesium at terapascal pressures, Nat. Phys. **18**, 1307 (2022).
[81] J. B. Neaton and N. W. Ashcroft, Pairing in dense lithium, Nature (London) **400**, 141 (1999).
[82] M. Hanfland, K. Syassen, N. E. Christensen, and D. L. Novikov, New high-pressure phases of lithium, Nature (London) **408**, 174 (2000).
[83] P. Li, G. Gao, Y. Wang, and Y. Ma, Crystal structures and exotic behavior of magnesium under pressure, J. Phys. Chem. C **114**, 21745 (2010).
[84] X. Dong *et al.*, A stable compound of helium and sodium at high pressure, Nat. Chem. **9**, 440 (2017).
[85] H. Zong, V. N. Robinson, A. Hermann, L. Zhao, S. Scandolo, X. Ding, and G. J. Ackland, Free electron to electride transition in dense liquid potassium, Nat. Phys. **17**, 955 (2021).
[86] S. Ahmed, F. González-Cataldo, V. N. Robinson, and B. Militzer, Electride behavior at high pressure in silicon and other elements in solid and liquid phases, Phys. Rev. B **112**, 165111 (2025).
[87] T. Guillot, The interiors of giant planets: Models and outstanding questions, Annu. Rev. Earth Planet Sci. **33**, 493 (2005).
[88] D. S. Spiegel, J. J. Fortney, and C. Sotin, Structure of exoplanets, Proc. Natl. Acad. Sci. U.S.A. **111**, 12622 (2014).
[89] R. Helled, N. Nettelmann, and T. Guillot, Uranus and neptune: Origin, evolution and internal structure, Space Sci. Rev. **216**, 38 (2020).
[90] S. Stanley and J. Bloxham, Convective-region geometry as the cause of Uranus' and Neptune's unusual magnetic fields, Nature (London) **428**, 151 (2004).
[91] M. Bethkenhagen, D. Cebulla, R. Redmer, and S. Hamel, Superionic phases of the 1:1 water-ammonia mixture, J. Phys. Chem. A **119**, 10582 (2015).
[92] T. Thévenet *et al.*, From methane to nanodiamond precursors in water: Superacid-like condensation pathways under extreme conditions, Angew. Chem., Int. Ed. Engl. **65**, e20364 (2025).
[93] F. Coppari, R. F. Smith, J. H. Eggert, J. Wang, J. R. Rygg, A. Lazicki, J. A. Hawreliak, G. W. Collins, and T. S. Duffy, Experimental evidence for a phase transition in magnesium oxide at exoplanet pressures, Nat. Geosci. **6**, 926 (2013).
[94] F. Coppari, R. F. Smith, J. Wang, M. Millot, D. Kim, J. R. Rygg, S. Hamel, J. H. Eggert, and T. S. Duffy, Implications of the iron oxide phase transition on the interiors of rocky exoplanets, Nat. Geosci. **14**, 121 (2021).
[95] Z. Konôpková, R. S. McWilliams, N. Gómez-Pérez, and A. F. Goncharov, Direct measurement of thermal conductivity in solid iron at planetary core conditions, Nature (London) **534**, 99 (2016).
[96] K. Ohta, Y. Kuwayama, K. Hirose, K. Shimizu, and Y. Ohishi, Experimental determination of the electrical resistivity of iron at Earth's core conditions, Nature (London) **534**, 95 (2016).
[97] M. Millot, N. Dubrovinskaia, A. Černok, S. Blaha, L. Dubrovinsky, D. G. Braun, P. M. Celliers, G. W. Collins, J. H. Eggert, and R. Jeanloz, Shock compression of stishovite and melting of silica at planetary interior conditions, Science **347**, 418 (2015).
[98] M. Guarguaglini, F. Soubiran, J.-A. Hernandez, A. Benuzzi-Mounaix, R. Bolis, E. Brambrink, T. Vinci, and A. Ravasio, Electrical conductivity of warm dense silica from double-shock experiments, Nat. Commun. **12**, 840 (2021).
[99] A. W. Ashley, M. Mookherjee, M. Xu, T. Yu, G. Manthilake, and Y. Wang, Viscosity measurements at high pressures: A critical appraisal of corrections to stokes' law, J. Geophys. Res. **129**, e2023JB028489 (2024).
[100] Anjeli Paola P. Estrada Alvarez *et al.*, Viscous motion of particles in shock-compressed epoxy, *Abstract submitted to the 65th Annual Meeting of the APS Division of Plasma Physics*, 2023, https://meetings-archive.aps.org/dpp/2023/cp11/64/.
[101] P. W. Hatfield *et al.*, The data-driven future of high-energy-density physics, Nature (London) **593**, 351 (2021).
[102] S. Jiang *et al.*, Thermal transport in warm dense matter revealed by refraction-enhanced x-ray radiography with a deep-neural-network analysis, Commun. Phys. **6**, 98 (2023).
[103] M. J. Guardalben, L. N. Goduguluri, A. Mathur, J. Wang, and R. Yadav, Prediction of laser beam spatial profiles in a high-energy laser facility by use of deep learning, Opt. Express **32**, 42692 (2024).
[104] L. Fiedler, K. Shah, M. Bussmann, and A. Cangi, Deep dive into machine learning density functional theory for materials science and chemistry, Phys. Rev. Mater. **6**, 040301 (2022).
[105] B. Huang, G. F. von Rudorff, and O. A. von Lilienfeld, The central role of density functional theory in the AI age, Science **381**, 170 (2023).
[106] *Foundation Models for Scientific Discovery and Innovation: Opportunities Across the Department of Energy and the Scientific Enterprise* (The National Academies Press, Washington, DC, 2025).